GEOPHYSICS, VOL. 84, NO. 3 (MAY-JUNE 2019); P. C171–C180, 10 FIGS., 1 TABLE.
10.1190/GEO2018-0300.1

Stacking-velocity tomography for tilted orthorhombic media

Qifan Liu[1] and Ilya Tsvankin[1]

ABSTRACT

Tilted orthorhombic (TOR) models are typical for dipping anisotropic layers, such as fractured shales, and can also be due to nonhydrostatic stress fields. Velocity analysis for TOR media, however, is complicated by the large number of independent parameters. Using multicomponent wide-azimuth reflection data, we develop stacking-velocity tomography to estimate the interval parameters of TOR media composed of homogeneous layers separated by plane dipping interfaces. The normal-moveout (NMO) ellipses, zero-offset traveltimes, and reflection time slopes of P-waves and split S-waves (S_1 and S_2) are used to invert for the interval TOR parameters including the orientation of the symmetry planes. We show that the inversion can be facilitated by assuming that the reflector coincides with one of the symmetry planes, which is a common geologic constraint often employed for tilted transversely isotropic media. This constraint makes the inversion for a single TOR layer feasible even when the initial model is purely isotropic. If the dip plane is also aligned with one of the symmetry planes, we show that the inverse problem for P-, S_1-, and S_2-waves can be solved analytically. When only P-wave data are available, parameter estimation requires combining NMO ellipses from a horizontal and dipping interface. Because of the increase in the number of independent measurements for layered TOR media, constraining the reflector orientation is required only for the subsurface layer. However, the inversion results generally deteriorate with depth because of error accumulation. Using tests on synthetic data, we demonstrate that additional information such as knowledge of the vertical velocities (which may be available from check shots or well logs) and the constraint on the reflector orientation can significantly improve the accuracy and stability of interval parameter estimation.

INTRODUCTION

Orthorhombic models are needed to adequately describe typical naturally fractured reservoirs and formations under nonhydrostatic stress, in particular near salt domes (Schoenberg and Helbig, 1997; Zhu et al., 2007; Tsvankin and Grechka, 2011; Jones and Davison, 2014, 2015). These models are often identified from the azimuthal variation of reflection moveout or from amplitude variation with offset and azimuth (Tsvankin and Grechka, 2011; Ravve and Koren, 2016).

Orthorhombic media are characterized by three mutually orthogonal symmetry planes (Figure 1). Tsvankin (1997) presents an extension of Thomsen (1986) parameters to orthorhombic symmetry using a limited equivalence between the symmetry planes of orthorhombic media and any plane of transversely isotropic (TI) models that contains the symmetry axis. Tsvankin's (1997) notation provides a convenient description of phase velocities and reflection seismic signatures both within and outside the symmetry planes.

Due to the dip of intrinsically anisotropic layers (e.g., shales) and properties of the stress field, none of the symmetry planes of orthorhombic models may be horizontal (Figure 2a). Because seismic data are usually acquired in the horizontal plane, such tilted orthorhombic (TOR) models create complicated seismic signatures that have to be taken into account in processing and inversion. The symmetry-plane orientation can be defined by the three Euler angles or, alternatively, by quaternions (Danek et al., 2013). Reconstruction of TOR models from seismic data is challenging because of the large number of independent parameters (Zhang and Zhang, 2012; Stovas, 2015; Ivanov and Stovas, 2016).

Normal-moveout (NMO) velocity is responsible for the most stable, conventional-offset portion of the moveout curve (i.e., for offsets limited by reflector depth) and can provide reliable information about subsurface velocity models (Tsvankin and Thomsen, 1994; Tsvankin, 2012). The azimuthal variation of NMO velocity of pure (nonconverted) modes in the acquisition plane is described by a

Manuscript received by the Editor 19 April 2018; revised manuscript received 15 November 2018; published ahead of production 07 February 2019; published online 10 April 2019.
[1]Colorado School of Mines, Golden, USA. E-mail: qifanliu@mines.edu; ilya@mines.edu.

quadratic form that typically represents an ellipse. The NMO ellipse is sensitive to the anisotropy coefficients and can be efficiently used in anisotropic velocity analysis (Tsvankin and Grechka, 2011).

Stacking-velocity tomography (Grechka et al., 2002a, 2002b) utilizes the NMO ellipses, zero-offset traveltimes, and reflection time slopes of pure modes (P, S_1, S_2) to perform parameter estimation in VTI (transversely isotropic with a vertical symmetry axis) and azimuthally anisotropic media. This inversion algorithm has been applied to layered models composed of tilted TI layers (Grechka et al., 2002a, 2002b; Wang and Tsvankin, 2010) and orthorhombic layers with a horizontal symmetry plane (Grechka et al., 2005). In particular, Grechka et al. (2005) demonstrate that the algorithm can successfully resolve the parameters of a dipping homogeneous orthorhombic layer with a horizontal symmetry plane when the reflector has a dip of at least 15°–20° and the dip plane deviates by more than 10° from the nearest symmetry plane. Constraints (e.g., those on the vertical velocities of P-, S_1-, and S_2-waves) are needed for stable inversion in layered orthorhombic media. The model obtained by stacking-velocity tomography can be refined using migration velocity analysis (e.g., Wang and Tsvankin, 2013). However, the properties of NMO ellipses in tilted orthorhombic media are more complicated (Ivanov and Stovas, 2016, 2017b), which hampers their application in velocity analysis.

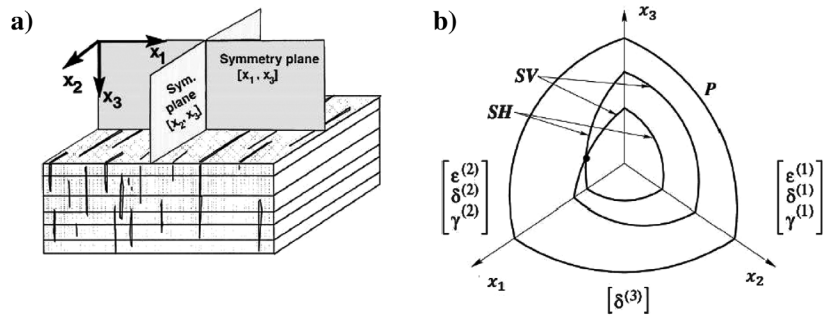

Figure 1. (a) Orthorhombic model caused by parallel vertical fractures embedded in a finely layered medium (Tsvankin, 1997). (b) Sketch of the phase-velocity surfaces and parameterization for orthorhombic media (Grechka et al., 1999). The anisotropy coefficients $\epsilon^{(i)}, \delta^{(i)}$, and $\gamma^{(i)}$ are defined in the corresponding symmetry planes (Tsvankin, 1997).

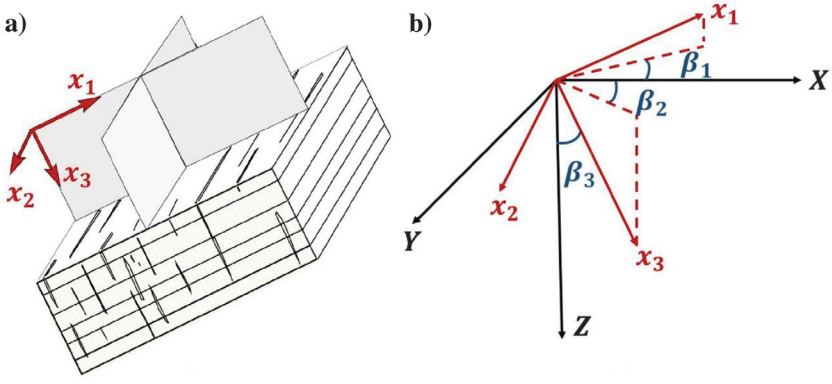

Figure 2. (a) Tilted orthorhombic model with the symmetry-plane orientation defined by the angles shown on plot (b). The angle β_1 is the azimuth of the x_1-axis of the orthorhombic model with respect to the global X-axis and β_2 and β_3 are the azimuth and the tilt of the x_3-axis of the orthorhombic model with respect to the global X- and Z-axes, respectively.

Here, we extend anisotropic stacking-velocity tomography to layered TOR models and discuss the feasibility of parameter estimation performed under different constraints. After describing the methodology, we analyze the inversion for a homogeneous TOR medium above a dipping interface and show that aligning the reflector with a symmetry plane makes the inverse problem unique. When only P-wave data are available, a subset of medium parameters can be estimated by adding reflections from a horizontal interface. Next, we demonstrate that the constraints on the reflector orientation become generally unnecessary for layered TOR models but help improve the inversion acuracy. Finally, numerical results illustrate the performance of the algorithm for noise-contaminated data from a stack of TOR layers separated by dipping interfaces.

THEORY

Parameterization

Here, we briefly review the parameterization and relevant properties of orthorhombic models. In the reference frame associated with the symmetry planes, orthorhombic media are defined by nine independent stiffness coefficients. Seismic signatures of orthorhombic models can be more conveniently described by the nine Tsvankin's (1997, 2012) parameters: the velocities V_{P0} and V_{S0} and anisotropy coefficients $\epsilon^{(1)}, \delta^{(1)}, \gamma^{(1)}$, $\epsilon^{(2)}, \delta^{(2)}, \gamma^{(2)}$, and $\delta^{(3)}$. Assuming that the symmetry planes are aligned with the Cartesian coordinate planes, V_{P0} and V_{S0} denote the velocities in the x_3-direction of the P-wave and of the split S-wave polarized in the x_1-direction. The superscripts denote the axis orthogonal to the plane in which each anisotropy coefficient is defined. For instance, the parameters $\epsilon^{(1)}, \delta^{(1)}$, and $\gamma^{(1)}$ are defined in the $[x_2, x_3]$-symmetry plane by analogy with Thomsen's VTI parameters.

The velocities and plane-wave polarizations in all symmetry planes can be obtained from the corresponding equations for TI media. For TOR models, the orientation of the symmetry planes can be specified by the Euler angles β_1, β_2, and β_3 (Figure 2b). The so-called singularity directions in which the phase velocities of the fast (S_1) and slow (S_2) shear waves coincide are not discussed here. (We assume that singularities are far enough from the zero-offset rays so that the fast and slow shear waves can be reliably separated for the range of source-receiver offsets sufficient to estimate NMO velocities. The shear wavefronts near point singularities are multivalued, have complicated shapes and cannot be accurately described by ray theory [Tsvankin and Grechka, 2011; Ivanov and Stovas, 2017a]).

We consider a stack of TOR layers separated by plane dipping interfaces (Figure 3) described by the distance D between the CMP location and the zero-offset reflection point, the azimuth of the dip plane (ψ), and the dip (ϕ). Hence, the model vector $\mathbf{m}$ for a dipping TOR layer includes 15 parameters:

$$\mathbf{m} = \{V_{P0}, V_{S0}, \epsilon^{(1)}, \delta^{(1)}, \gamma^{(1)}, \epsilon^{(2)}, \delta^{(2)}, \gamma^{(2)}, \delta^{(3)}, \beta_1, \beta_2, \beta_3, D, \psi, \phi\}. \quad (1)$$

NMO ellipse in anisotropic media

As demonstrated by Grechka and Tsvankin (1998), the NMO velocity of any pure mode in arbitrarily anisotropic, heterogeneous media can be represented as the following function of azimuth α:

$$V_{\rm nmo}^{-2}(\alpha) = W_{11}\cos^2\alpha + 2W_{12}\sin\alpha\cos\alpha + W_{22}\sin^2\alpha, \quad (2)$$

where $\mathbf{W}$ is a 2×2 symmetric matrix controlled by the slowness surface near the slowness direction of the zero-offset ray.

Typically, the matrix $\mathbf{W}$ has positive eigenvalues and $V_{\rm nmo}(\alpha)$ is described by an ellipse. There are exceptions (not addressed here) for uncommon geologic structures in which the CMP traveltime either does not increase with offset or cannot be described by a hyperbolic equation even for small offset-to-depth ratios (Tsvankin, 2012).

For a single homogeneous layer, the matrix $\mathbf{W}$ can be found as (Grechka et al., 1999):

$$\mathbf{W} = f(p_1, p_2, q) = \frac{p_1 q_{,1} + p_2 q_{,2} - q}{q_{,11}q_{,22} - q_{,12}^2}\begin{pmatrix} q_{,22} & -q_{,12} \\ -q_{,12} & q_{,11}\end{pmatrix}, \quad (3)$$

where $(p_1, p_2, q = p_3)$ are the components of the slowness vector $\mathbf{p}$ of the zero-offset ray, $q_{,i} \equiv \partial q/\partial p_i$, and $q_{,ij} \equiv \partial^2 q/(\partial p_i \partial p_j)$; $q_{,i}$ and $q_{,ij}$ are defined for the slowness direciton of the zero-offset ray. The slowness components satisfy the Christoffel equation $\Gamma(p_1, p_2, q) = 0$, where Γ is a six-order polynomial in q. The derivatives $q_{,i}$ and $q_{,ij}$ can be obtained using implicit differentiation as (Grechka et al., 1999):

$$q_{,i} = -\frac{\Gamma_{p_i}}{\Gamma_q} \quad (4)$$

and

$$q_{,ij} = -\frac{\Gamma_{p_i p_j} + \Gamma_{p_i q} q_{,j} + \Gamma_{p_j q} q_{,i} + \Gamma_{qq} q_{,i} q_{,j}}{\Gamma_q}, \quad (5)$$

where $\Gamma_{p_i} \equiv \partial\Gamma/\partial p_i$, $\Gamma_q \equiv \partial\Gamma/\partial q$, $\Gamma_{p_i p_j} \equiv \partial^2\Gamma/(\partial p_i \partial p_j)$, $\Gamma_{p_i q} \equiv \partial^2\Gamma/(\partial p_i \partial q)$, and $\Gamma_{qq} \equiv \partial^2\Gamma/\partial q^2$.

The effective matrix $\mathbf{W}$ for layered models can be computed by applying Dix-type averaging of the interval $\mathbf{W}$-matrices, as discussed by Grechka and Tsvankin (2002a) and Tsvankin and Grechka (2011). It is possible to compute the NMO ellipse of any reflection event by tracing just the zero-offset ray and calculating the corresponding slowness vector along with the derivatives of the vertical slowness with respect to the horizontal slowness components.

Stacking-velocity tomography

Stacking-velocity tomography is a two-stage iterative inversion scheme for estimating the interval medium parameters and reconstructing the model interfaces (reflectors). Introduced for anisotropic media by Grechka et al. (2002a, 2002b), it operates with normal-moveout velocity (which is usually close to the stacking velocity) estimated on conventional CMP spreads. This algorithm can be applied to multicomponent wide-azimuth reflection data to obtain a more complete set of medium parameters compared to P-wave inversion (Grechka et al., 2002b, 2005; Tsvankin and Grechka, 2011).

The input data for 3D stacking-velocity tomography include the one-way zero-offset reflection traveltimes τ_0, the horizontal slownesses p_1 and p_2 which can be estimated from reflection time slopes (Grechka et al., 2002a, 2002b; Tsvankin and Grechka, 2011), and the effective NMO ellipses. Thus, each mode ($\rm P, S_1, S_2$) contributes six measurements to the data vector which includes 18 elements per layer:

$$\mathbf{d}(Q, \mathbf{Y}) = \{\tau_0(\mathbf{Y}), p_{1,Q}(\mathbf{Y}), p_{2,Q}(\mathbf{Y}), W_{11,Q}(\mathbf{Y}), W_{12,Q}(\mathbf{Y}), W_{22,Q}(\mathbf{Y})\}, \quad (6)$$

where Q denotes the mode, and $\mathbf{Y}$ is the CMP location. In practice, the traveltimes τ_0 and NMO ellipses (matrices $\mathbf{W}$) are usually obtained from 3D semblance analysis, while the horizontal slownesses p_1 and p_2 are found from reflection slopes on the zero-offset (or stacked) time section (Grechka et al., 2002a, 2002b).

Although the input data are supposed to include all three pure-mode reflections ($\rm P, S_1, S_2$), it may not be necessary to generate shear waves. Grechka and Tsvankin (2002b) show that the traveltime of any primary SS ($\rm S_1S_1$ or $\rm S_2S_2$) reflection from a certain interface can be obtained using the traveltimes of the corresponding PP and PS reflections (the so-called PP + PS = SS method). Grechka and Dewangan (2003) further demonstrate that the kinematically accurate SS primary reflections can be generated by using a specific convolution

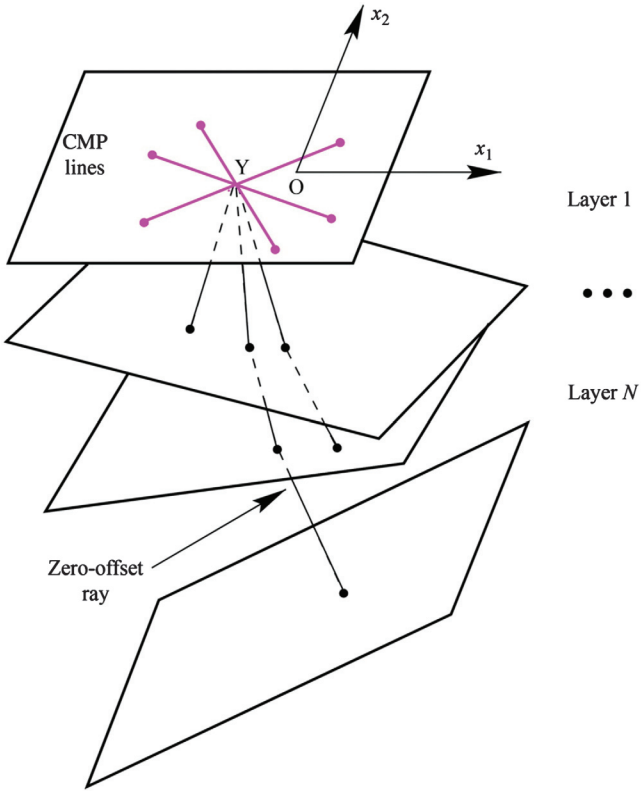

Figure 3. Multiazimuth CMP gather and zero-offset rays propagating in a stack of TOR layers separated by plane dipping interfaces (after Grechka et al., 2002a).

of the windowed PP and PS seismograms. The PP + PS = SS method does not require precise velocity information and can be applied before anisotropic velocity model-building.

Stacking-velocity tomography includes the following steps:

1) Estimate the data vector **d** (equation 6) for available reflection events.
2) Build (at the first iteration) or update the trial model **m**.
3) Compute zero-offset rays for all available events and reconstruct reflectors for the trial model.
4) Compute the effective NMO ellipses (matrices **W**).
5) Evaluate the objective function (see below).
6) Obtain the inversion gradients and update the model (back to the second step).

The inversion starts by defining a trial set of the interval parameters and computing the vertical slowness of the zero-offset ray in the subsurface layer for each pure mode using the horizontal slownesses obtained from the reflection time slopes. The full slowness vector and zero-offset traveltime are used to trace each downgoing zero-offset ray, find the zero-offset reflection point and the corresponding reflector normal, and reconstruct the reflecting interface (Figure 3). Once a complete trial model has been built, one can compute the NMO ellipses for all available events and update the parameters by minimizing the difference between the computed and observed NMO ellipses (Grechka et al., 2002a). It should be emphasized that the effective matrix **W** can be obtained by tracing a single (zero-offset) ray, which makes this scheme computationally efficient. The objective function for multicomponent tomography also includes the differences between the reflector depths obtained from different modes:

$$\mathcal{F}(\mathbf{m}) = \sum_{i,j=1,2} \left\| 1 - \frac{W_{ij}^{\mathrm{cal}}(\mathbf{m})}{W_{ij}^{\mathrm{obs}}} \right\| + \alpha \left\| 1 - \frac{z_Q(\mathbf{m})}{z_{Q'}(\mathbf{m})} \right\|, \quad (7)$$

where $\mathbf{W}^{\mathrm{cal}}(\mathbf{m})$ describes the NMO ellipses of the pure modes (P, S_1, S_2) calculated for the trial model **m**, $\mathbf{W}^{\mathrm{obs}}$ corresponds to the NMO ellipses estimated from the reflection data, and $z_Q(\mathbf{m})$ and $z_{Q'}(\mathbf{m})$ are the reflector depths at the CMP location computed for modes Q and Q' [the ratios $z_Q/z_{Q'}$ are computed for each pair of the modes - $(\mathrm{P}, \mathrm{S}_1)$, $(\mathrm{P}, \mathrm{S}_2)$, and $(\mathrm{S}_1, \mathrm{S}_2)$].

Numerical tests show that values of the weighting factor α between 0.5 and 1.0 generally yield satisfactory results for TOR media; α is set to 0.5 in all examples below. We use the Gauss-Newton method to solve this nonlinear inverse problem, with the model parameters updated by iterative minimization of the objective function (equation 7). Although our methodology can account for reflector curvature in the computation of effective NMO ellipses (see Blias, 2009; Tsvankin and Grechka, 2011), the scope of this paper is limited to layered TOR models with planar interfaces.

PARAMETER ESTIMATION FOR A SINGLE TOR LAYER

We begin with the model of a single homogeneous TOR layer above a dipping reflector. As shown below, not all elements of the data vector for this model are independent, but the inversion becomes feasible using certain constraints on the orientation of the symmetry planes. Analytic results are confirmed by numerical tests for noise-contaminated data.

As mentioned above, the model vector **m** for a dipping TOR layer includes 15 parameters (equation 1). If all components of **d** were independent, the inversion for the TOR parameters and interfaces would be overdetermined. However, as discussed below, the number of independent components of the data vector depends on the specific type of TOR media.

According to Snell's law, the slowness vector of the zero-offset ray of any pure mode should be perpendicular to the reflector. Therefore, although each mode Q may have a different group-velocity direction, the slowness (or phase-velocity) vectors $\{p_{1,Q}, p_{2,Q}, q_{1,Q}\}$ of the zero-offset rays in a single layer are parallel to each other. As a result, the ratio p_1/p_2 is the same for all three modes and determines the azimuth (ψ) of the dip plane of the reflector (i.e., the vertical plane that contains the reflector normal). This means there are only four independent elements in the six-dimensional $(p_{1,Q}, p_{2,Q})$ vector of the horizontal slownesses for the P-, S_1-, and S_2-waves. For instance, given the ratio $r = p_{2,P}/p_{1,P}$ for the P-wave and the component p_{1,S_1} for the S_1-wave, the component p_{2,S_1} can be found as $p_{1,\mathrm{S}_1} r$.

Also, the zero-offset traveltimes of the three modes ($\tau_{0,Q}$) constrain only one combination of the model parameters. Grechka et al. (2005) show that for a planar reflector with the normal **n** defined in the Cartesian coordinate system by $\mathbf{n} \cdot \mathbf{x} = D$, the ratio $\tau_{0,Q}/p_{1,Q}$ is equal to $D/\sin\phi$ for all modes. Therefore, the zero-offset times of the three modes provide only one independent measurement. As a result, the data vector for a single TOR layer contains 14 independent elements:

$$\mathbf{d} = \{\tau_{0,P}, p_{1,P}, p_{1,\mathrm{S}_1}, p_{1,\mathrm{S}_2}, p_{2,P}, W_{11,Q}, W_{12,Q}, W_{22,Q}\}. \quad (8)$$

Because the number of medium parameters exceeds the number of measurements, it is necessary to impose constraints to overcome the ambiguity of the inverse problem.

1. Reflector co-oriented with a symmetry plane

In many cases of practical importance, one of the symmetry planes of TOR media is co-oriented with the reflector beneath it. This constraint is often used for dipping shale layers described by a tilted TI medium with the symmetry axis orthogonal to the reflector (Charles et al., 2008; Wang and Tsvankin, 2013). If the shale contains parallel fractures orthogonal to the layer boundaries, such model becomes titled orthorhombic with a symmetry plane that coincides with the reflector.

For this model, the local axis x_3 of the TOR medium is orthogonal to the reflector, which means that $\beta_2 = \psi$ and $\beta_3 = \phi$. Our numerical testing also shows that in this case the parameter $\delta^{(3)}$ has no influence on the NMO ellipses and, therefore, is not relevant in NMO-velocity inversion. In principle, it may be possible to estimate $\delta^{(3)}$ from the P-wave nonhyperbolic moveout (Tsvankin and Grechka, 2011). Then the model vector contains just 12 independent elements:

$$\mathbf{m} = (V_{P0}, V_{S0}, \epsilon^{(1)}, \delta^{(1)}, \gamma^{(1)}, \epsilon^{(2)}, \delta^{(2)}, \gamma^{(2)}, D, \beta_1, \psi, \phi). \quad (9)$$

Next, we discuss two cases corresponding to different mutual orientations of the dip plane of the reflector and the symmetry planes of the medium.

1.1 Dip plane co-oriented with a symmetry plane

If one of the symmetry planes of the TOR medium coincides with the dip plane of the reflector beneath it, the dip plane becomes a plane of symmetry for the entire model and the NMO ellipses of all three modes have the same orientation (Figure 4a). This orientation (azimuth ψ) can be found using the horizontal slownesses p_1 and p_2 of any mode ($\tan\psi = p_2/p_1$). If the coordinate axes are aligned with the dip and strike directions, the matrix element $W_{12} = 0$. The elements W_{11} and W_{22} can be obtained by analogy with TI media because the reflections recorded on the dip and strike lines propagate in the $[x_1, x_3]$ and $[x_2, x_3]$ symmetry planes.

For the strike-line reflection, the model is equivalent to a VTI medium above a horizontal reflector (Grechka and Tsvankin, 1998). Assuming that the fast S-wave propagating in the x_3-direction of the orthorhombic model is polarized along the x_2-axis (which implies that $\gamma^{(1)} > \gamma^{(2)}$), the velocities of the fast (V_{S1}) and slow (V_{S2}) shear waves in the x_3-direction can be written as:

$$V_{S1} = V_{S0}\sqrt{\frac{1+2\gamma^{(1)}}{1+2\gamma^{(2)}}}, \quad V_{S2} = V_{S0}. \quad (10)$$

Then the NMO velocities are given by:

$$V^{(1)}_{\mathrm{nmo},P} = V_{P0}\sqrt{1+2\delta^{(1)}}, \quad (11)$$

$$V^{(1)}_{\mathrm{nmo},S1} = V_{S1}\sqrt{1+2\sigma^{(1)}}, \quad (12)$$

$$V^{(1)}_{\mathrm{nmo},S2} = V_{S2}\sqrt{1+2\gamma^{(1)}} = V_{S1}\sqrt{1+2\gamma^{(2)}}, \quad (13)$$

where

$$\sigma^{(1)} \equiv (V_{P0}/V_{S1})^2\,(\epsilon^{(1)} - \delta^{(1)}). \quad (14)$$

For the reflection on the dip line, the model is equivalent to a TI medium with the symmetry axis parallel to the reflector normal (Tsvankin, 2012). Then, the dip-line NMO velocities take the form:

$$V^{(2)}_{\mathrm{nmo},P} = V_{P0}\sqrt{1+2\delta^{(2)}}/\cos\phi, \quad (15)$$

$$V^{(2)}_{\mathrm{nmo},S1} = V_{S1}\sqrt{1+2\gamma^{(2)}}/\cos\phi = V^{(1)}_{\mathrm{nmo},S2}/\cos\phi, \quad (16)$$

$$V^{(2)}_{\mathrm{nmo},S2} = V_{S2}\sqrt{1+2\sigma^{(2)}}/\cos\phi, \quad (17)$$

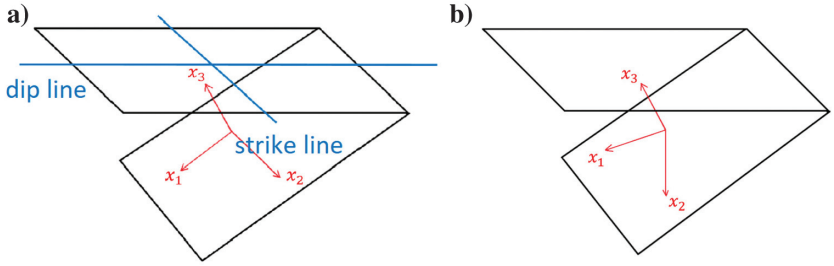

Figure 4. Models with the reflector that coincides with the $[x_1, x_2]$ symmetry plane of the orthorhombic medium above it. (a) The dip plane coincides with the $[x_1, x_3]$ symmetry plane (b). The dip plane has arbitrary orientation.

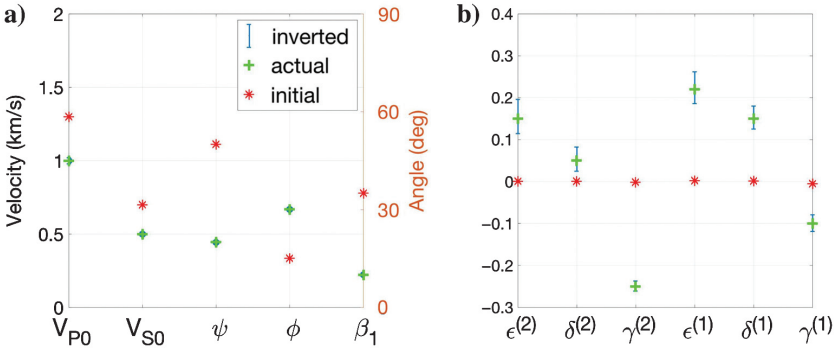

Figure 5. Inversion of noise-contaminated data for a single TOR layer. The reflector coincides with the $[x_1, x_2]$ symmetry plane of the medium. The inversion is repeated 100 times with different realizations of noise (see the main text). The error bars here (and in Figures 7–10) mark the standard deviations of the inverted parameters.

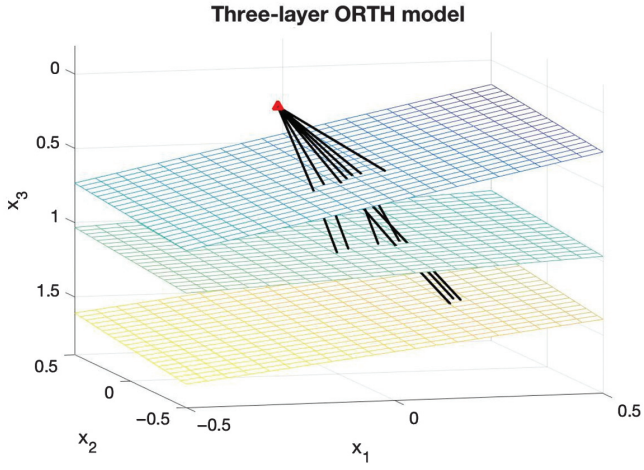

Figure 6. Zero-offset rays in a model composed of three TOR layers separated by plane dipping interfaces. Each reflector coincides with a symmetry plane of the medium above it. Therefore, the zero-offset rays for all modes in the layer above the reflector are parallel to the reflector normal. As a result, the zero-offset rays of the P-, S_1- and S_2-waves reflected from the bottom of the near-surface layer are parallel to one another. Due to the transmission through the intermediate interfaces, the zero-offset rays of different modes from the two deeper reflectors deviate from one another at the surface.

where

$$\sigma^{(2)} \equiv (V_{P0}/V_{S2})^2\ (\epsilon^{(2)} - \delta^{(2)}). \tag{18}$$

Because of the symmetry of this model, the zero-offset rays and the corresponding phase and group velocities are parallel to the x_3-direction of the TOR medium. Hence, the horizontal slowness $p_{\mathrm{hor,Q}}$ (horizontal projection of the slowness vector) of each mode can be expressed as:

$$p_{\mathrm{hor,Q}} \equiv \sqrt{p_{1,Q}^2 + p_{2,Q}^2} = \frac{\sin\phi}{V_{Q0}}, \tag{19}$$

where V_{Q0} represents the phase and group velocity in the x_3-direction of the corresponding mode ($V_{Q0} = V_{P0}, V_{S1}, V_{S2}$).

According to equation 16, the combination of the NMO velocities $V^{(2)}_{\mathrm{nmo},S1}$ and $V^{(1)}_{\mathrm{nmo},S2}$ yields the reflector dip ϕ. Next, the x_3-direction velocities V_{P0}, V_{S1}, and V_{S2} can be calculated from the estimated dip and the corresponding horizontal slownesses (equation 19). Finally, the anisotropy coefficients $\delta^{(1)}$, $\gamma^{(1)}$, $\epsilon^{(1)}$, $\delta^{(2)}$, $\gamma^{(2)}$, and $\epsilon^{(2)}$ are obtained from equations 10–18.

In addition, because V_{Q0} represents the group velocity of the zero-offset ray, the distance D between the CMP and the zero-offset reflection point can be found using the one-way zero-offset time $\tau_{0,Q}$ as:

$$D = V_{Q0}\,\tau_{0,Q} \quad (Q = P, \mathrm{S}_1, \mathrm{S}_2). \tag{20}$$

Therefore, equations 10–20 make it possible to obtain all layer parameters analytically, making numerical inversion unnecessary.

If only P-wave data are available, equations 10, 15, and 19 are insufficient for resolving the parameters V_{P0}, $\delta^{(1)}$, $\delta^{(2)}$, and ϕ. However, the inversion becomes possible by combining the NMO ellipses from a horizontal and dipping reflector. In particular, the combination of fault-plane reflections and subhorizontal events is often used in anisotropic velocity analysis (Alkhalifah and Tsvankin, 1995; Stunff et al., 2001; Tsvankin and Grechka, 2011). Also, reflections from two different dips can be generated by bending shale layers, which are common in fold-and-thrust belts (Tsvankin and Grechka, 2011). Wide-azimuth P-wave reflections from a horizontal interface beneath an orthorhombic medium provide the zero-dip NMO velocities $V^{(1)}_{\mathrm{nmo},P}$ and $V^{(2)}_{\mathrm{nmo},P}$. Then, the reflector dip can be estimated from the dip-line NMO velocity of the dipping event (equation 15), which makes it possible to find V_{P0} from equation 19. Finally, the coefficients $\delta^{(1)}$ and $\delta^{(2)}$ are obtained from the velocities $V^{(1)}_{\mathrm{nmo},P}$ and $V^{(2)}_{\mathrm{nmo},P}$.

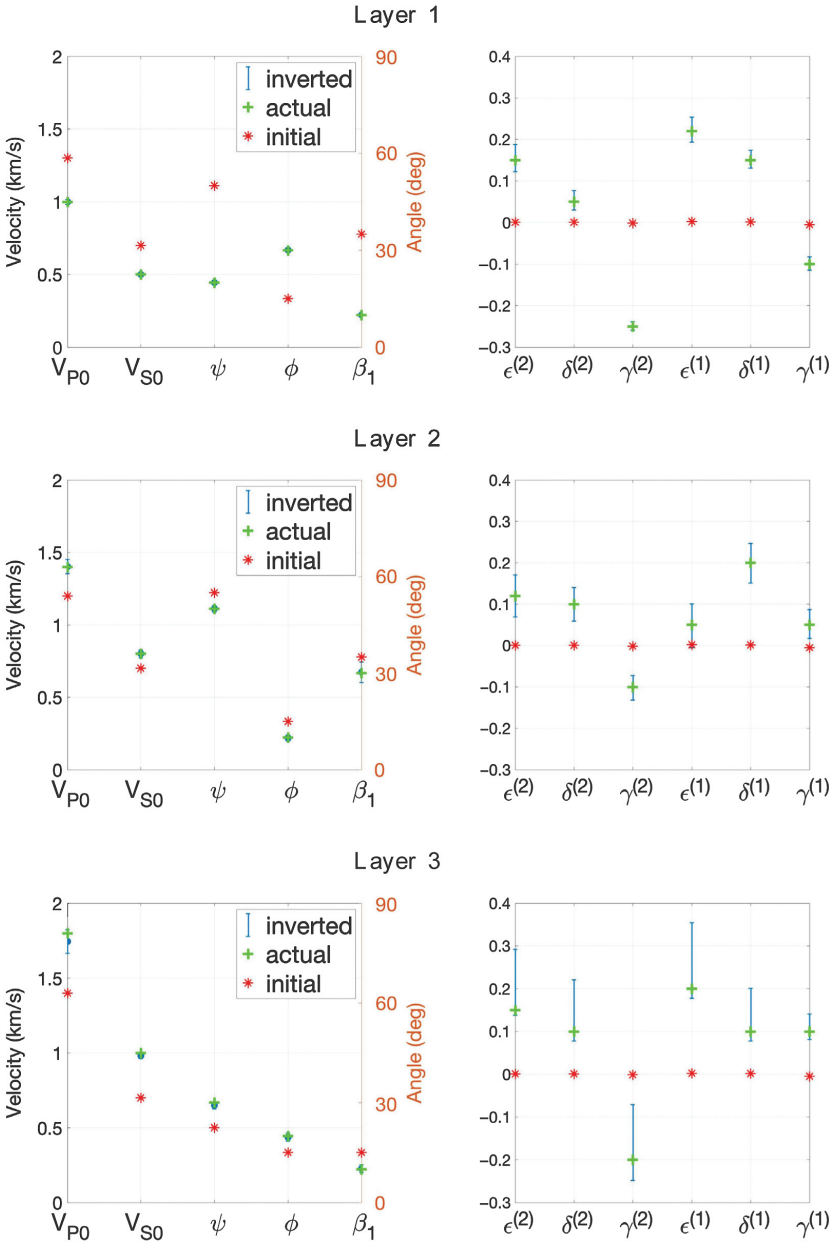

Figure 7. Inversion of noise-contaminated data for a three-layer TOR model. All interfaces coincide with the $[x_1, x_2]$ symmetry plane of the medium above it. Input data are contaminated with Gaussian noise that has a standard deviation of 1% for the zero-offset traveltimes and horizontal slownesses and 2% for the matrix elements W_{ij} responsible for the NMO ellipses.

1.2 Arbitrary dip-plane orientation

If the dip plane of the reflector does not coincide with any of the symmetry planes (Figure 4b), the NMO ellipses of different modes do not have the same orientation. Also, none of the ellipses is generally co-oriented with the dip plane, so the matrix elements W_{ij} for each mode are independent and, in general, do not vanish (equations 8 and 9). Then, the number of independent measurements (14) exceeds the number of model parameters (12), making the inversion potentially possible.

Still, the feasibility of this nonlinear multiparameter inverse problem needs to be examined on

noise-contaminated data. We contaminate input data with Gaussian noise that has a standard deviation of 1% for the zero-offset traveltimes and horizontal slownesses and 2% for the matrix elements W_{ij} responsible for the NMO ellipses. The inversion is repeated 100 times for different realizations of the noise. The inversion results (Figure 5) show that the algorithm converges towards the true model and remains stable even when the initial model is isotropic with the P- and S-wave velocities that deviate by about 20% from the actual values. The standard deviations of the inverted parameters are listed below (Table 1). The algorithm accurately estimates the velocities V_{P0}, V_{S0}, and orientation angles, and provides reasonably tight constraints on the relevant anisotropy coefficients.

When the dip plane of the reflector deviates from the symmetry planes of the TOR medium, the P-wave NMO ellipse is influenced by two additional anisotropy parameters, $\epsilon^{(1)}$ and $\epsilon^{(2)}$, and the symmetry-plane azimuth β_1 (Figure 2b). Therefore, the combination of P-wave reflections from a horizontal and dipping interface is no longer sufficient for parameter estimation without additional constraints.

2. Arbitrary reflector orientation

If neither the reflector itself nor its dip plane coincide with a symmetry plane of the layer, the model vector consists of 15 parameters (equation 1).

Because the data in this model provide only 14 independent measurements (equation 8), the inverse problem is underdetermined and does not have a unique solution.

PARAMETER ESTIMATION FOR LAYERED MEDIA

The above analysis for a homogeneous TOR medium provides important insights into the potential for reconstructing layered orthorhombic models from reflection data. Here, stacking-velocity tomography is tested on a three-layer TOR medium in Figure 6.

It is important to note that the relationships between the data-vector elements described above for a single layer hold only for the subsurface layer. The slowness directions of different modes are governed by the interval parameters and Snell's law at the medium interfaces. Hence, the slowness vectors of the zero-offset rays of the P-, S_1-, and S_2-waves reflected from the second and third interfaces (Figure 6) are no longer parallel at the observation surface, so the ratios p_1/p_2 are different. Likewise, the zero-offset times of the deeper events (P, S_1, S_2) provide independent information for the inversion. This means that the data vector for the reflections from the second or deeper interfaces includes 18 independent measurements (equation 6).

1. Reflector co-oriented with a symmetry plane

First, we assume that each reflector coincides with a symmetry plane of the medium above it. The tomographic algorithm performs

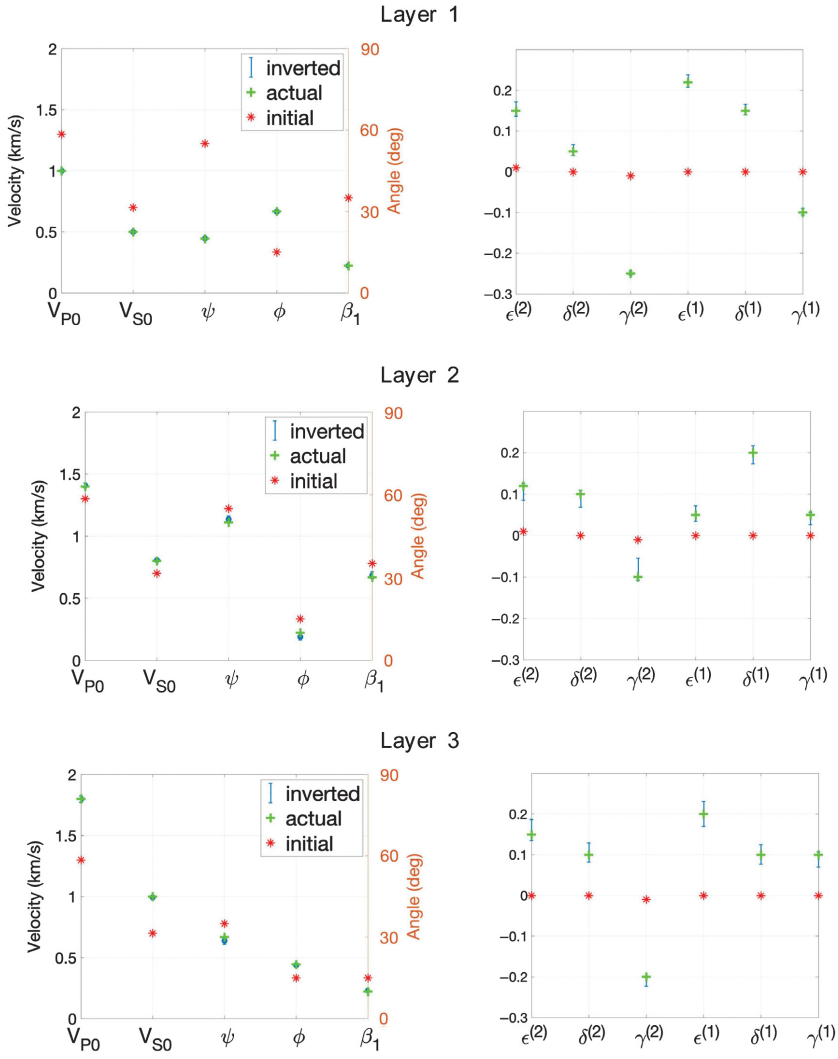

Figure 8. Inversion of noise-contaminated data with vertical-velocity constraints (equation 21). All interfaces coincide with the $[x_1, x_2]$ symmetry plane of the medium above it. Input data are contaminated with Gaussian noise that has a standard deviation of 1% for the zero-offset traveltimes and horizontal slownesses and 2% for the elements W_{ij}.

Table 1. Standard deviations of the inverted parameters for the model in Figure 5.

Parameter	V_{P0} (km/s)	V_{S0} (km/s)	$\beta_3(\psi)$	$\beta_2(\phi)$	β_1	$\epsilon^{(2)}$	$\delta^{(2)}$	$\gamma^{(2)}$	$\epsilon^{(1)}$	$\delta^{(1)}$	$\gamma^{(1)}$
Actual value	1.00	0.50	20°	30°	10°	0.15	0.05	−0.25	0.22	0.15	−0.10
Standard deviation	0.03	0.02	0.83°	2.19°	1.85°	0.04	0.03	0.01	0.04	0.03	0.02

the inversion in a layer-stripping fashion followed by "global" optimization that involves the entire set of interval parameters. During layer stripping, the parameters of the shallowest layer are estimated first and used to invert for the parameters of the second layer, and the procedure continues downward. Then the results are refined by simultaneously inverting for all interval TOR parameters.

Our numerical results show that if the input data are noise-free, stacking-velocity tomography can accurately recover all interval medium parameters (except for $\delta^{(3)}$) and reconstruct the interfaces. However, the results are hampered by error accumulation with depth. Relatively small errors in the shallow layers may get significantly amplified in the deeper part of the model (Figure 7). To make the inversion more stable, we impose constraints on the interval vertical velocities in each layer by adding another term to the objective function:

$$\mathcal{F}'(\mathbf{m}) = \mathcal{F}(\mathbf{m}) + \alpha' \left\| 1 - \frac{V^{\text{cal}}_{Q,\text{vert}}(\mathbf{m})}{V^{\text{obs}}_{Q,\text{vert}}} \right\|, \qquad (21)$$

where $\mathcal{F}(\mathbf{m})$ is from equation 7, $V^{\text{cal}}_{Q,\text{vert}}(\mathbf{m})$ are the vertical group velocities for the trial model $\mathbf{m}$, and $V^{\text{obs}}_{Q,\text{vert}}$ are the actual velocities (Q corresponds to waves P, S_1, and S_2). It should be mentioned that the vertical group velocities differ from V_{P0}, V_{S0}, and V_{S1} when the orthorhombic model does not have a horizontal symmetry plane. The velocities $V^{\text{cal}}_{Q,\text{vert}}$ are calculated for the trial model, whereas $V^{\text{obs}}_{Q,\text{vert}}$ are assumed to be available from borehole data (Wang and Tsvankin, 2013). The weighting factor α' is set to 0.5 for all numerical tests below.

Parameter estimation is performed 100 times with different realizations of the noise. The initial models for all three TOR layers are purely isotropic. We put constraints on the interval vertical group velocities ($V_{P,\text{vert}}$, $V_{S_1,\text{vert}}$, and $V_{S_2,\text{vert}}$) in all layers according to equation 21. The observed velocities are computed as random values that deviate by less than 1% from the actual velocities. Although the inversion errors slightly increase with depth, the algorithm remains stable and gives sufficiently accurate estimates of the interval parameters (Figure 8).

In the next test, we increase the magnitude of the noise, which now has a standard deviation of 2% for the zero-offset traveltimes and horizontal slownesses and 5% for the matrix elements W_{ij} (Figure 9). Despite the larger uncertainty in the input data, the inverted velocities and orientation angles are estimated with sufficient accuracy, while the errors in the anisotropy coefficients somewhat increase. Still, the inversion provides useful information about the interval parameters of the layered TOR medium.

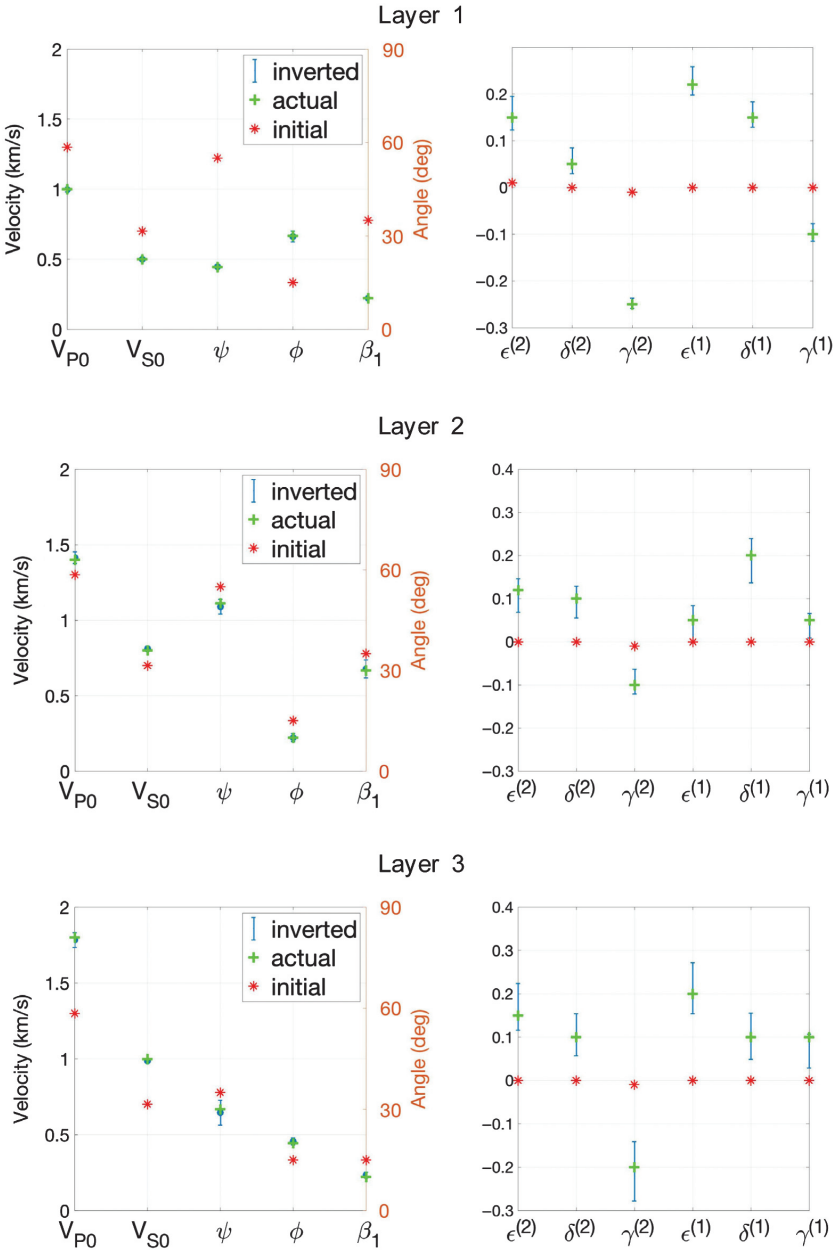

Figure 9. Same as Figure 8 but the input data are contaminated with Gaussian noise that has a standard deviation of 2% for the zero-offset traveltimes and horizontal slownesses and 5% for the elements W_{ij}.

2. Arbitrary reflector orientation

If the reflector is not co-oriented with any of the symmetry planes of the TOR medium above it, the vector of the interval parameters includes 15 elements (equation 21). As discussed earlier, the data vector provides 18 independent measurements for the second or deeper layers, making the inversion for TOR models with arbitrarily oriented reflectors potentially feasible.

However, error accumulation with depth and the trade-offs among parameters may cause substantial distortions in the inversion results. Therefore, a priori constraints are essential in making the inversion sufficiently stable. In particular, our numerical testing shows that the vertical-velocity constraints introduced above (equation 21) help resolve the interval parameters (Figure 10). The results, however, are less accurate compared to

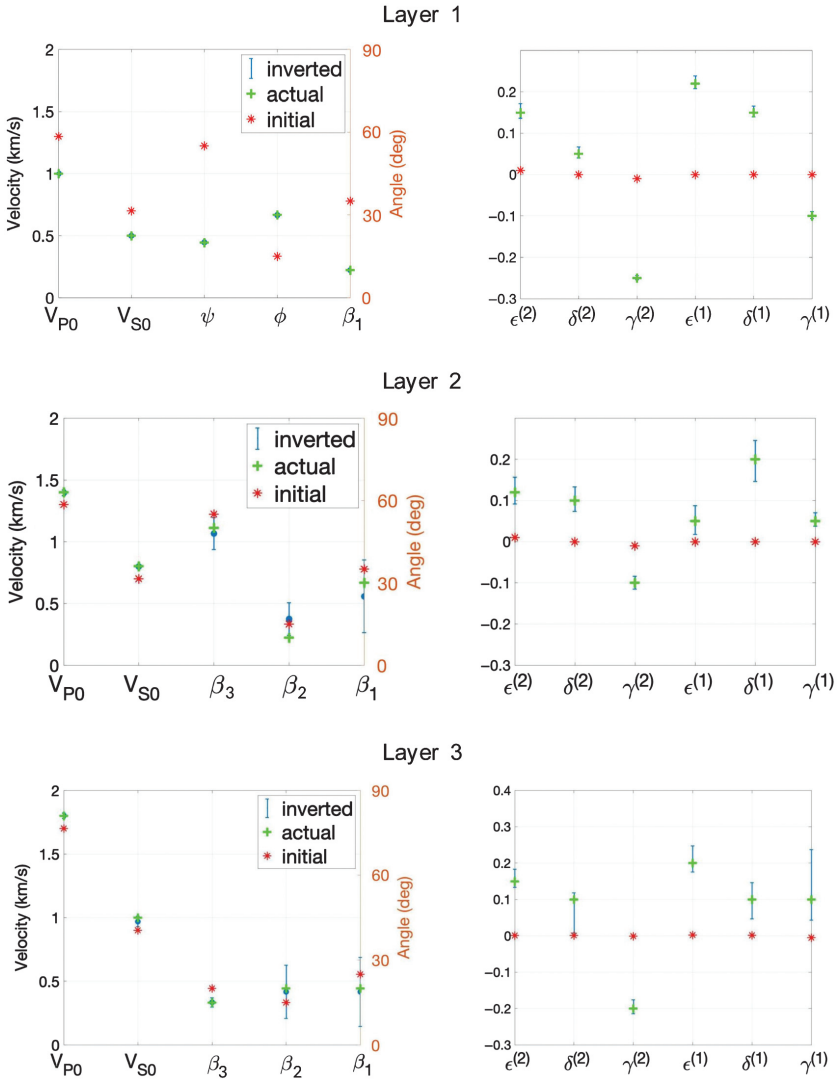

Figure 10. Inversion of noise-contaminated data with vertical-velocity constraints for a three-layer TOR model. The first interface coincides with the $[x_1, x_2]$ symmetry plane of the shallowest layer, while the deeper interfaces are not aligned with symmetry planes. Input data are contaminated with Gaussian noise that has a standard deviation of 1% for the zero-offset traveltimes and horizontal slownesses and 2% for the elements W_{ij}.

those for models in which each reflector is aligned with a symmetry plane of the medium above it. This is likely due to the additional ambiguity caused by the need to estimate the two extra angles that define the reflector normal.

CONCLUSIONS

Parameter estimation for tilted orthorhombic (TOR) media may play an important role in characterizing naturally fractured reservoirs and building accurate velocity models for subsalt exploration. We demonstrate that parameters of layered TOR media can be reconstructed from 3D wide-azimuth conventional-spread reflection data under certain constraints. The normal-moveout (NMO) ellipses, zero-offset traveltimes, and reflection time slopes of P-waves and split S-waves (S_1 and S_2) are used to invert for the interval TOR parameters along with the layer boundaries. Because the NMO ellipses can be obtained by tracing only zero-offset rays, this scheme is computationally efficient. Although the algorithm operates with pure-mode reflections, the input S-wave data can be generated by the PP + PS = SS method that does not require shear-wave excitation.

To make the inversion for a single TOR layer feasible, it is necessary to assume that the reflector coincides with a symmetry plane of the medium. If the dip plane of the reflector is aligned with another symmetry plane and all three modes (P, S_1, S_2) are available, the problem can be solved analytically (the only unconstrained parameter in this case is $\delta^{(3)}$, the Thomsen-style δ-coefficient defined in the reflector plane). When only P-wave data are recorded, the pertinent medium parameters and reflector dip ϕ can be found by combining reflections from a horizontal and dipping interface. For reflectors with arbitrary dip-plane orientation, we perform numerical tests on noise-contaminated P-, S_1-, and S_2-data. The results show that the inversion remains stable even if the initial model is isotropic with significantly distorted velocities.

For layered TOR media, it may not be necessary to impose constraints on the reflector orientation in the second or deeper layers. However, our numerical analysis shows that to mitigate error accumulation with depth, it is highly beneficial to constrain the vertical velocities using well logs or VSP (vertical seismic profiling) data. On the whole, the developed inversion scheme can be efficiently used to build initial TOR models for anisotropic reflection tomography or full-waveform inversion.

ACKNOWLEDGMENTS

This work was supported by the Consortium Project on Seismic Inverse Methods for Complex Structures at the Center for Wave Phenomena (CWP). We are grateful to V. Grechka (Marathon Oil) and A. Pech (Smart Ray Geosolutions) for making available their modeling codes. We also thank members of the A(nisotropy)-Team at CWP for numerous helpful discussions. The paper greatly benefited from detailed and insightful comments of the reviewers (especially Y. Ivanov and A. Stovas) and editors D. Draganov and I. Ravve.

DATA AND MATERIALS AVAILABILITY

Data associated with this research are available and can be obtained by contacting the corresponding author.

REFERENCES

Alkhalifah, T., and I. Tsvankin, 1995, Velocity analysis for transversely isotropic media: Geophysics, **60**, 1550–1566, doi: 10.1190/1.1443888.

Blias, E., 2009, Stacking velocities in the presence of overburden velocity anomalies: Geophysical Prospecting, **57**, 323–341, doi: 10.1111/j.1365-2478.2008.00750.x.

Charles, S., D. R. Mitchell, R. A. Holt, J. Lin, and J. Mathewson, 2008, Data-driven tomographic velocity analysis in tilted transversely isotropic media: A 3D case history from the Canadian foothills: Geophysics, **73**, no. 5, VE261–VE268, doi: 10.1190/1.2952915.

Danek, T., M. Kochetov, and M. A. Slawinski, 2013, Uncertainty analysis of effective elasticity tensors using quaternion-based global optimization and Monte-Carlo method: The Quarterly Journal of Mechanics and Applied Mathematics, **66**, 253–272, doi: 10.1093/qjmam/hbt004.

Grechka, V., and P. Dewangan, 2003, Generation and processing of pseudo-shear-wave data: Theory and case study: Geophysics, **68**, 1807–1816, doi: 10.1190/1.1635033.

Grechka, V., A. Pech, and I. Tsvankin, 2002a, Multicomponent stacking-velocity tomography for transversely isotropic media: Geophysics, **67**, 1564–1574, doi: 10.1190/1.1512802.

Grechka, V., A. Pech, and I. Tsvankin, 2002b, P-wave stacking-velocity tomography for VTI media: Geophysical Prospecting, **50**, 151–168, doi: 10.1046/j.1365-2478.2002.00307.x.

Grechka, V., A. Pech, and I. Tsvankin, 2005, Parameter estimation in orthorhombic media using multicomponent wide-azimuth reflection data: Geophysics, **70**, no. 2, D1–D8, doi: 10.1190/1.1897026.

Grechka, V., and I. Tsvankin, 1998, 3-D description of normal-moveout in anisotropic inhomogeneous media: Geophysics, **63**, 1079–1092, doi: 10.1190/1.1444386.

Grechka, V., and I. Tsvankin, 2002a, NMO-velocity surfaces and Dix-type formulas in anisotropic heterogeneous media: Geophysics, **67**, 939–951, doi: 10.1190/1.1484536.

Grechka, V., and I. Tsvankin, 2002b, PP + PS = SS: Geophysics, **67**, 1961–1971, doi: 10.1190/1.1527096.

Grechka, V., I. Tsvankin, and J. K. Cohen, 1999, Generalized Dix equation and analytic treatment of normal-moveout velocity for anisotropic media: Geophysical Prospecting, **47**, 117–148, doi: 10.1046/j.1365-2478.1999.00120.x.

Ivanov, Y., and A. Stovas, 2016, Normal-moveout velocity ellipse in tilted orthorhombic media: Geophysics, **81**, no. 6, C319–C336, doi: 10.1190/geo2016-0143.1.

Ivanov, Y., and A. Stovas, 2017a, S-wave singularities in tilted orthorhombic media: Geophysics, **82**, no. 4, WA11–WA21, doi: 10.1190/geo2016-0642.1.

Ivanov, Y., and A. Stovas, 2017b, Traveltime parameters in tilted orthorhombic media: Geophysics, **82**, no. 6, C187–C200, doi: 10.1190/geo2016-0486.1.

Jones, I. F., and I. Davison, 2014, Seismic imaging in and around salt bodies: Interpretation, **2**, no. 4, SL1–SL20, doi: 10.1190/INT-2014-0033.1.

Jones, I. F., and I. Davison, 2015, Seismic imaging in and around salt bodies — Problems and pitfalls update: 77th Annual International Conference and Exhibition, EAGE, Extended Abstracts, WS12-B03, doi: 10.1190/segam2014-0047.1.

Ravve, I., and Z. Koren, 2016, Normal moveout velocity for pure-mode and converted waves in layered orthorhombic media: Geophysical Prospecting, **64**, 1235–1258, doi: 10.1111/1365-2478.12340.

Schoenberg, M., and K. Helbig, 1997, Orthorhombic media: Modeling elastic wave behavior in a vertically fractured earth: Geophysics, **62**, 1954–1974, doi: 10.1190/1.1444297.

Stovas, A., 2015, Azimuthally dependent kinematic properties of orthorhombic media: Geophysics, **80**, no. 6, C107–C122, doi: 10.1190/geo2015-0288.1.

Stunff, Y. L., V. Grechka, and I. Tsvankin, 2001, Depth-domain velocity analysis in VTI media using surface P-wave data: Is it feasible?: Geophysics, **66**, 897–903, doi: 10.1190/1.1444979.

Thomsen, L., 1986, Weak elastic anisotropy: Geophysics, **51**, 1954–1966, doi: 10.1190/1.1442051.

Tsvankin, I., 1997, Anisotropic parameters and P-wave velocity for orthorhombic media: Geophysics, **62**, 1292–1309, doi: 10.1190/1.1444231.

Tsvankin, I., 2012, Seismic signatures and analysis of reflection data in anisotropic media, 3rd ed.: SEG.

Tsvankin, I., and V. Grechka, 2011, Seismology of azimuthally anisotropic media and seismic fracture characterization: SEG.

Tsvankin, I., and L. Thomsen, 1994, Nonhyperbolic reflection moveout in anisotropic media: Geophysics, **59**, 1290–1304, doi: 10.1190/1.1443686.

Wang, X., and I. Tsvankin, 2010, Stacking-velocity inversion with borehole constraints for tilted TI media: Geophysics, **75**, no. 5, D69–D77, doi: 10.1190/1.3481652.

Wang, X., and I. Tsvankin, 2013, Ray-based gridded tomography for tilted transversely isotropic media: Geophysics, **78**, no. 1, C11–C23, doi: 10.1190/geo2012-0066.1.

Zhang, H. J., and Y. Zhang, 2011, Reverse time migration in vertical and tilted orthorhombic media: 81st Annual International Meeting, SEG, Expanded Abstracts, 185–189, doi: 10.1190/1.3627568.

Zhu, T., S. H. Gray, and D. Wang, 2007, Prestack Gaussian-beam depth migration in anisotropic media: Geophysics, **72**, no. 3, S133–S138, doi: 10.1190/1.2711423.